© 2014. Published by The Company of Biologists Ltd | Development (2014) 141, 1064-1074 doi:10.1242/dev.097774

RESEARCH ARTICLE

Microtubule-severing protein Katanin regulates neuromuscular junction development and dendritic elaboration in *Drosophila*

Chuan-Xi Mao[1,2], Ying Xiong[2], Zhaohuan Xiong[1], Qifu Wang[2], Yong Q. Zhang[2,*] and Shan Jin[1,*]

ABSTRACT

Microtubules (MTs) are crucial for diverse biological processes including cell division, cell growth and motility, intracellular transport and the maintenance of cell shape. MT abnormalities are associated with neurodevelopmental and neurodegenerative diseases such as hereditary spastic paraplegia. Among many MT regulators, katanin was the first identified MT-severing protein, but its neuronal functions have not yet been examined in a multicellular organism. Katanin consists of two subunits; the catalytic subunit katanin 60 contains an AAA (ATPases associated with a variety of cellular activities) domain and breaks MT fibers while hydrolyzing ATP, whereas katanin 80 is a targeting and regulatory subunit. To dissect the *in vivo* functions of Katanin, we generated mutations in *Drosophila Katanin 60* and manipulated its expression in a tissue-specific manner. Null mutants of *Katanin 60* are pupal lethal, demonstrating that it is essential for viability. Loss-of-function mutants of *Katanin 60* showed excess satellite boutons, reduced neurotransmission efficacy, and more enlarged cisternae at neuromuscular junctions. In peripheral sensory neurons, loss of *Katanin 60* led to increased elaboration of dendrites, whereas overexpression of *Katanin 60* resulted in the opposite. Genetic interaction analyses indicated that increased levels of MT acetylation increase its susceptibility to Katanin-mediated severing in neuronal and non-neuronal systems. Taken together, our results demonstrate for the first time that Katanin 60 is required for the normal development of neuromuscular synapses and dendrites.

KEY WORDS: *Drosophila melanogaster*, Katanin, Spastin, HDAC6, Neuromuscular junction

INTRODUCTION

Microtubules (MTs) play a crucial role in a diverse array of fundamental cellular processes including cell division, cell growth and the maintenance of cell shape. MT dynamics are tightly regulated by a host of proteins that stabilize or destabilize MTs. Three MT-severing proteins, katanin, spastin and fidgetin, are members of the diverse ATPases associated with a variety of cellular activities (AAA) protein superfamily (Roll-Mecak and McNally, 2010; Sharp and Ross, 2012). Katanin, the founding member of the MT-severing protein family, was initially identified from *Xenopus* egg extracts exhibiting MT-severing activity (Vale, 1991). It consists of two subunits, katanin 60 and katanin 80 (McNally and Vale, 1993). Katanin 60 is the catalytic subunit that breaks MT fibers while hydrolyzing ATP, whereas katanin 80 is a targeting and regulatory subunit (Hartman and Vale, 1999).

[1]College of Life Science, Hubei University, Wuhan, Hubei 430062, China. [2]Key Laboratory of Molecular and Developmental Biology, Institute of Genetics and Developmental Biology, Chinese Academy of Sciences, Beijing 100101, China.

*Authors for correspondence (yqzhang@genetics.ac.cn; jinshan@hubu.edu.cn)

Received 20 April 2013; Accepted 22 December 2013

The *in vivo* functions of katanin 60 have been characterized in a range of organisms. Genetic analyses of katanin 60 in *Tetrahymena* showed that it plays a crucial role in the formation of cilia and is essential for locomotion (Sharma et al., 2007). *Caenorhabditis elegans* mutant for the *katanin 60* homolog *mei-1* show meiotic spindle abnormalities (Srayko et al., 2006). In *Drosophila* S2 cells, overexpression of Katanin 60 results in MT severing and depolymerization (Díaz-Valencia et al., 2011; Zhang et al., 2007; Zhang et al., 2011). The susceptibility of MTs to katanin-mediated severing is controlled by many factors; for example, acetylation of MTs sensitizes their severing by katanin (Sudo and Baas, 2010) whereas tau binding to MTs protects them from katanin severing (Qiang et al., 2006; Qiang et al., 2010; Sudo and Baas, 2010; Yu et al., 2008).

Katanin is distributed in all neuronal compartments including axons, dendrites and cell bodies, and is particularly abundant in axons, whereas spastin is mostly concentrated at axonal branching points (Ahmad et al., 1999; Karabay et al., 2004; Sharp and Ross, 2012; Yu et al., 2008). In the rodent brain, katanin levels are high during rapid phases of axonal growth but diminish as axons reach their targets (Karabay et al., 2004). In cultured rat sympathetic neurons, expression of a dominant-negative form of katanin 60 inhibits MT severing and axonal growth, whereas overexpression of wild-type katanin 60 results in excess MT severing, but can also be deleterious to axonal growth in a subset of neurons (Karabay et al., 2004). Thus, katanin is a crucial regulator of axonal growth.

Dendrites play an essential role in information processing in the nervous system as they are involved in synapse formation and signal integration (Jan and Jan, 2010). MTs are crucial for dendrite elaboration. However, how MT regulators including MT-severing proteins affect dendritic development is poorly understood.

Previous studies have uncovered an important role for spastin in neuromuscular junction (NMJ) growth and dendritic elaboration (Jinushi-Nakao et al., 2007; Ozdowski et al., 2011; Trotta et al., 2004; Sherwood et al., 2004; Yao et al., 2011; Ye et al., 2011). However, how katanin affects neuronal development has not been characterized at an organism level. To dissect the neuronal function of katanin we generated mutants of *Drosophila melanogaster Katanin 60* and transgenic lines that could be used to overexpress Katanin 60 in a tissue-specific manner. We then examined the effects of altered Katanin 60 expressions on NMJ synapses, neuronal morphogenesis and the MT cytoskeleton. We report for the first time that Katanin 60 is required for the normal development of NMJs and dendrites in *Drosophila*.

RESULTS

The *Drosophila* genome encodes an ortholog of human katanin 60

Sequence comparisons revealed that the *Drosophila* genome contains a gene that encodes an ortholog of human katanin 60. *Drosophila* Katanin 60 protein is overall 50% identical and 63%

Development (2014) doi:10.1242/dev.097774

similar to human katanin 60 (Fig. 1A). The identity and similarity of the AAA domains of the two homologs are 80% and 93%, respectively. Indeed, katanin 60 is well conserved from *C. elegans* to humans, and the high degree of homology suggests that katanin 60 function has been conserved through evolution.

As a first step to understanding the *in vivo* function of Katanin 60 we generated two deletions, *77* and *721*, which remove the N-terminus of Katanin 60 (Fig. 1B), by imprecise excision of the *P*-element insertion *EY09078*. We also used ends-out targeting to produce deletion *17A* that deletes 252 amino acids containing the entire AAA domain in the Katanin 60 C-terminus (Fig. 1A,B). These deletions are likely to be nulls because there was no detectable protein as evaluated by western blotting with an antibody against Katanin 60 (Fig. 1C). Immunostaining with the antibody detected no specific signals of endogenous Katanin 60 in the ventral nerve cord, NMJs and sensory neurons of wild-type larvae, but cytoplasmic Katanin 60 was observed when it was neuronally overexpressed driven by *elav-Gal4* or *ppk-Gal4* (Fig. 1D; supplementary material Fig. S1). Heteroallelic *77*, *721* and *17A* combinations or hemizygous mutants that carry each of the deletions on one chromosome and the deficiency *Df(3R)ED5138* that removes the entire *Katanin 60* gene on the other, were all early pupal lethal. Specifically, 80% of homozygous *Katanin* 60^{17A} mutants died at larval stages, whereas the remaining 20% lived to early pupal stage. The surviving mutant larvae appeared sluggish. As a control, the precise excision line 66 was fully viable as either homozygous or hemizygous over *Df(3R)ED5138*.

To determine whether the mutant phenotype could be rescued by re-expression of Katanin 60, we generated multiple transgenic lines carrying *UAS-Katanin 60* insertions at 51D through site-directed integration (Bischof et al., 2007) as well as at non-targeted sites. Ubiquitous and neuronal overexpression of *Katanin 60* in *Katanin* 60^{17A} background by *da-Gal4* and *elav-Gal4*, respectively, delayed the lethality of mutants to adult stage. More importantly, one or two copies of the targeted *UAS-Katanin 60* insertion without *Gal4* drivers but not the original *ZH-attP-51D* line effectively rescued the lethality of homozygous *Katanin* 60^{17A} mutants to adulthood, suggesting that a low-level expression of Katanin 60 from the targeted UAS insertion as detected by western analysis (Fig. 2H) is sufficient to rescue the lethality.

Katanin 60 regulates NMJ synapse development

Misregulated MTs lead to abnormal NMJ synapses in *Drosophila* (Jin et al., 2009; Nahm et al., 2013; Roos et al., 2000; Ruiz-Canada et al., 2004; Sherwood et al., 2004; Trotta et al., 2004; Wang et al., 2007; Yao et al., 2011; Zhang et al., 2001). To determine whether Katanin 60 plays a role in synapse development, we co-stained larval NMJs with anti-horseradish peroxidase (HRP) to reveal the neuronal membrane, and with anti-cysteine string protein (CSP) to label synaptic vesicles. Striking NMJ abnormalities were observed in *Katanin* 60^{17A} mutants (Fig. 2). Wild-type synaptic boutons were arranged in a linear 'beads-on-a-chain' pattern, but synaptic boutons in homozygous and hemizygous *Katanin* 60^{17A} mutants were obviously smaller and more numerous (Fig. 2B,C). We quantified the number of total boutons and satellite boutons of NMJ 4 from the abdominal segment A3. The number of total boutons was significantly increased from 25.2±0.72 in wild type to 33.35±1.43 in homozygous *Katanin* 60^{17A} mutants (P<0.001), as was the number of satellite boutons from 1.35±0.37 in wild type to 9.45±0.87 in homozygous *Katanin* 60^{17A} mutants (Fig. 2B,F,G). Satellite boutons are defined as a bouton of smaller size than the adjacent mature boutons along NMJ branches (Dickman et al., 2006). The satellite boutons started to form

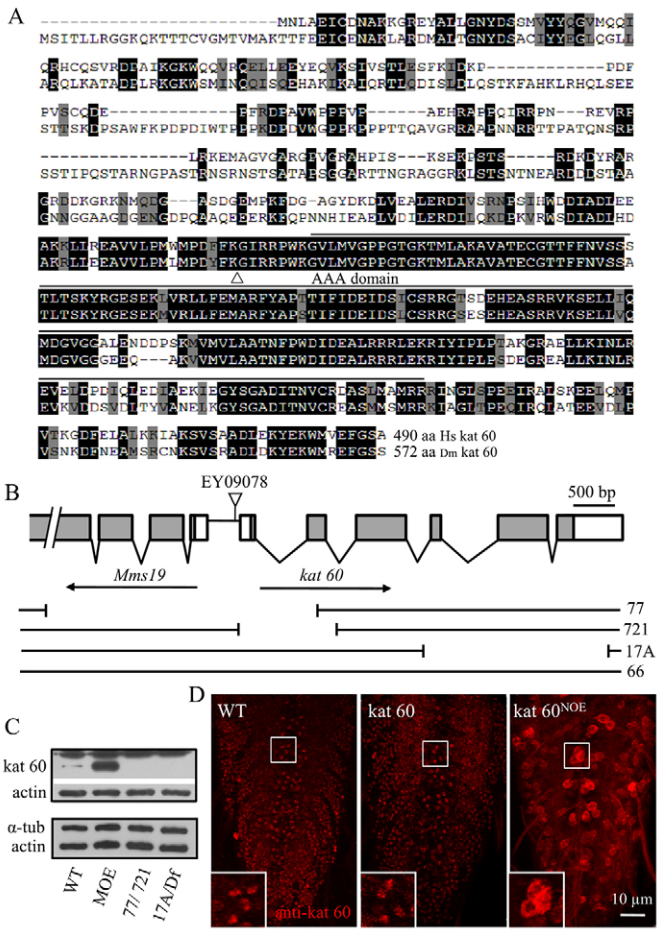

Fig. 1. *Drosophila* Katanin 60. (A) Sequence alignment of *Drosophila* (Dm kat) and human (Hs kat) katanin 60. The AAA domain is delineated as previously published (Hartman and Vale, 1999). Black and gray shading indicate identical and similar amino acids, respectively. The triangle indicates the site at which deletion 17A starts. (B) Genomic structure of *Drosophila Katanin 60* and mapping of mutants. The intron-exon organization of *Katanin 60* and its flanking gene, *Mms19*, is shown at the top. The orientation of the *Katanin 60* locus is opposite to that of the third chromosome. Gray boxes, coding regions; white boxes, untranslated regulatory regions; gaps, introns; horizontal line, intergenic region. Deletions 77, 721 and 17A are depicted, as is the precise excision line 66. (C) Western analysis of larval carcasses with anti-Katanin 60 recognizing the N-terminus of Katanin 60. No Katanin 60 was observed in *Katanin* 60^{17A} mutants. No change in α-tubulin (α-tub) protein levels was detected when *Katanin 60* expression was altered. MOE, muscular overexpression of Katanin 60 from the targeted UAS insertion driven by *C57-Gal4*; Df, *Df(3R)ED5138*. Actin was used as a loading control. (D) Katanin 60 is cytoplasmic. No specific Katanin 60 expression was detected in the ventral ganglions of wild-type larvae. However, cytoplasmic Katanin 60 was detected in neurons when Katanin 60 was overexpressed, driven by *elav-Gal4*. WT, wild type; NOE, neuronal overexpression. Scale bar: 10 µm.

in the middle third instar larval stages of *Katanin* 60^{17A} mutants (supplementary material Fig. S2). The excess number of total boutons, largely due to the formation of satellite boutons, was also present in *Katanin* 60^{17A} hemizygous larvae which carry the *17A* deletion on one chromosome and *Df(3R)ED5138* on the other (P<0.001; Fig. 2C,F,G). The excess of satellite boutons was highly penetrant and was also observed in other NMJs such as NMJ6/7 of homozygous and hemizygous *Katanin* 60^{17A} mutants.

To confirm that loss of Katanin 60 produced the observed NMJ alterations, we carried out rescue experiments by expressing *Katanin*

Development (2014) doi:10.1242/dev.097774

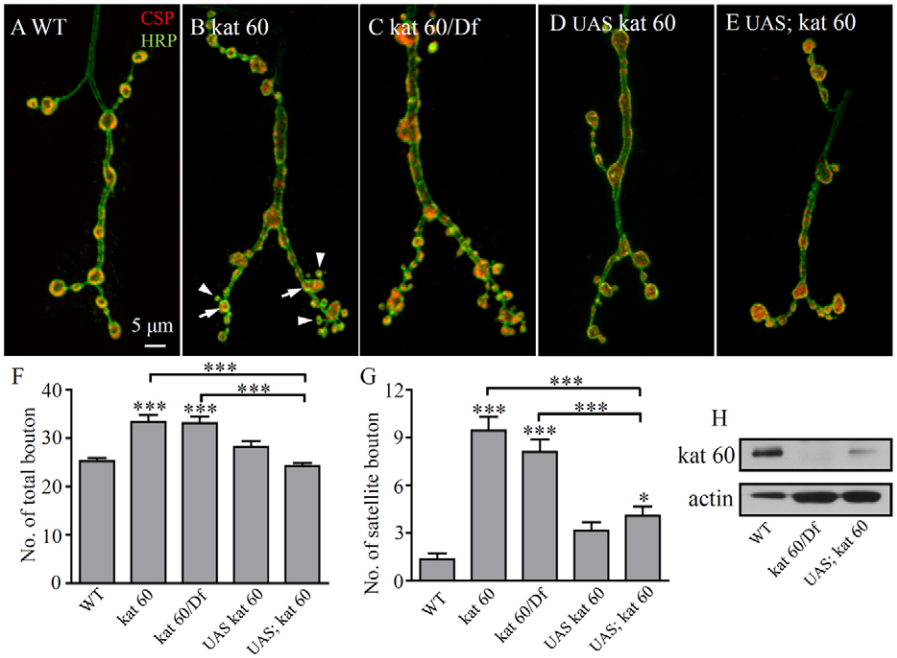

Fig. 2. Katanin 60 regulates NMJ synapse development. (A-E) NMJs from wandering third instar larvae double-stained with anti-HRP (green) and anti-CSP (red). Representative muscle 4 NMJs of the abdominal segment A3 are shown for wild type (A), *Katanin 60^{17A}* (B), *Katanin 60^{17A}/Df(3R)ED5138* (C), homozygous targeted *UAS-Katanin 60* insertion without a Gal4 driver (D), and homozygous *UAS-Katanin 60* insertion in a *Katanin 60^{17A}* background (E). Scale bar: 5 µm. Arrows and arrowheads in B indicate synaptic and satellite boutons, respectively. (F,G) Quantification of the total number of boutons (F) and satellite boutons (G) from different genotypes (n=20 NMJs). *P<0.05, ***P<0.001. Error bars indicate s.e.m. (H) Western analysis of larval carcasses with anti-Katanin 60. A low level of Katanin 60 was detected from homozygous *UAS-Katanin 60* insertion at 51D without Gal4 drivers in the *Katanin 60^{17A}* background. Five times more protein was loaded for the two mutant genotypes than the wild type. Actin was used as a loading control.

60 in the *Katanin 60^{17A}* background. Overexpression of *Katanin 60* driven by the pan-neuronal *elav-Gal4*, the muscle-specific *C57-Gal4*, or the ubiquitous *da-Gal4* in the mutant background showed no rescue of the *Katanin 60^{17A}* NMJ phenotypes. This is not surprising as overexpression of *Katanin 60* from multiple independent *UAS* lines by *elav-Gal4* in the wild-type background produced NMJ phenotypes with more satellite boutons, whereas muscular overexpression of *Katanin 60* by *C57-Gal4* had a minor effect on NMJ growth (see below in Fig. 6). However, as with the lethality rescue shown above, heterozygous or homozygous targeted *UAS-Katanin 60* insertion without Gal4 drivers rescued the excess satellite boutons of homozygous (Fig. 2E-G) and hemizygous (data not shown) *Katanin 60^{17A}* mutants, whereas the original *ZH-attP-51D* line did not. As a control, the number of satellite boutons in NMJ terminals of the homozygous *UAS-Katanin 60* line was as in the wild type (Fig. 2D). The excess satellite boutons in homozygous, hemizygous and trans-allelic *Katanin 60* mutants, together with the effective rescue of the phenotypes by a low-level expression of Katanin 60, demonstrate that loss of Katanin 60 specifically causes the prominent NMJ phenotypes.

Increased Futsch-positive loops in the NMJ terminals of *Katanin 60* mutants

To evaluate the effects of Katanin 60 on MTs at NMJ synapses, we stained NMJ terminals with antibodies against Futsch, the *Drosophila* ortholog of microtubule-associated protein MAP1B (Hummel et al., 2000; Zhang et al., 2001), and α-tubulin. At the wild-type muscle 4 NMJ, continuous MT bundles run along the NMJ axes. MTs within boutons are occasionally arranged in loops. MT loops are associated with an arrest in synaptic bouton division, whereas irregular and branched MT arrays indicate an actively growing or budding bouton (Conde and Cáceres, 2009). There were significantly more Futsch-positive MT loops in *Katanin 60^{17A}* NMJ terminals than in controls (P<0.001; Fig. 3A,B,E). A homozygous *UAS-Katanin 60* insertion fully reversed the effect on the MT loops in *Katanin 60^{17A}* mutants to the wild-type level (Fig. 3C,E). Overexpression of Katanin 60 in wild-type background by *elav-Gal4* did not alter the number of Futsch-positive loops at NMJs (Fig. 3D,E). Using anti-α-tubulin staining, we were able to clearly see more MT loops within synaptic boutons of *Katanin 60^{17A}* mutants than the wild type (Fig. 3F-G″). When *Katanin 60* was overexpressed in presynaptic neurons by *elav-Gal4*, we observed short MT fragments within the terminal boutons (Fig. 3I-I″). MTs within synaptic boutons of different genotypes are schematically presented in Fig. 3F″-I″.

The ultrastructure of NMJ synapses is altered in *Katanin 60* mutants

To investigate further the effects of Katanin 60 on the structure of NMJ synapses, we examined larval NMJ6 and 7 by electron microscopy (Fig. 4A-G). The most common organelles in wild-type NMJ are active zones, mitochondria, and small clear-core synaptic vesicles 35-50 nm in diameter. The profile of presynaptic boutons containing active zones of transmitter release in *Katanin 60^{17A}* mutants appeared largely normal (Fig. 4A,B). We detected no obvious alterations in presynaptic T-bars, postsynaptic densities, or the subsynaptic reticulum (SSR) (Fig. 4A,B,D,E). However, a large number of enlarged vesicles up to 200 nm in diameter were observed throughout the boutons of *Katanin 60^{17A}* animals (Fig. 4B,F-H). Some of the large vesicles were horse-shoe shaped (Fig. 4F,G). There were ten times more enlarged vesicles, with diameter ≥80 nm, in the NMJ boutons of *Katanin 60^{17A}* mutants than the wild type (P<0.001; Fig. 4A,B,F-H). Homozygous *UAS-Katanin 60* insertion fully rescued the enlarged vesicle phenotype of *Katanin 60^{17A}* mutants (Fig. 4C,H), indicating that the increased number of cisternae at NMJs is specifically caused by *Katanin 60* mutations. How Katanin 60 affects cisterna formation in the NMJs remains unknown at present. However, we note that the other MT-severing protein spastin affects vesicle formation by interacting with integral membrane proteins or membrane-associated proteins (Blackstone et al., 2011).

Katanin 60 is required for normal neurotransmission at NMJ synapses

Given the morphological and structural abnormalities in NMJs of *Katanin 60* mutants (Figs 2, 3), synaptic transmission might be also defective. To test this possibility we examined both evoked and spontaneous synaptic glutamate release using intracellular recordings

Development (2014) doi:10.1242/dev.097774

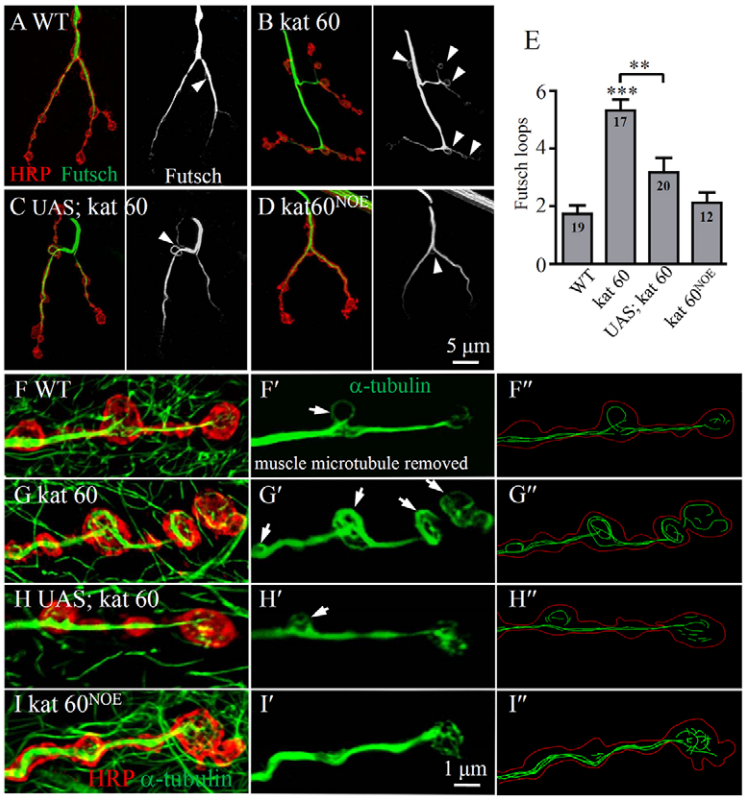

Fig. 3. Increased Futsch-positive MT loops in NMJ terminals of *Katanin 60* null mutants. (A-D) NMJ terminals of wild type (A), *Katanin 60*^{17A} (B), homozygous *UAS-Katanin 60* insertion in a *Katanin 60*^{17A} background (C), and neuronal overexpression of *Katanin 60* by *elav-Gal4* (D), co-stained with anti-HRP (red) and anti-Futsch (green). Futsch-positive loops are indicated by arrowheads. Scale bar: 5 µm. (E) Statistical comparison of the number of Futsch-positive loops at the NMJ terminals in different genotypes. The number of NMJs analyzed for each genotype is given on the bars. ***P*<0.01, ****P*<0.001; error bars indicate s.e.m. (F-I) NMJ terminals of different genotypes co-stained with anti-HRP (red) and anti-α-tubulin (green). (F′-I′) For better visualization of the MT cytoskeleton in NMJ terminals, MT staining in muscles was removed from single confocal slices before projection of serial images. MT loops are indicated by arrows. Scale bar: 1 µm. (F″-I″) MTs within synaptic boutons of different genotypes are depicted with Imaris.

from muscle 6 in the abdominal segment A3. Compared with the wild type, *Katanin 60*^{17A} mutants showed a significant decrease in excitatory junctional potential (EJP) amplitudes (*P*<0.001; Fig. 5A,B). The decreased EJP amplitudes in *Katanin 60*^{17A} mutants were partially rescued by one copy, and completely rescued to wild-type levels by two copies, of the *UAS-Katanin 60* insertion (Fig. 5C,D).

We also examined miniature EJPs (mEJPs), i.e. the postsynaptic response to a spontaneous single-vesicle release. The mEJP amplitudes, also known as quantal size, of *Katanin 60*^{17A} mutants were not significantly different from those of the wild type (Fig. 5A-C,E). The mEJP frequency in *Katanin 60*^{17A} mutants, however, was significantly decreased by 37% compared with wild type (*P*<0.01). The decreased mEJP frequency was rescued by heterozygous (*P*<0.05) and homozygous *UAS-Katanin 60* insertions (*P*<0.001; Fig. 5A-C,F). Because the evoked EJP amplitudes were decreased, whereas the mEJP amplitudes were normal in *Katanin* mutants, quantal content (QC; the number of vesicles released per evoked event), calculated by dividing the corrected EJP amplitude by the mEJP amplitude, was reduced to 51% of the wild-type level (*P*<0.01) (Fig. 5G). A single copy of the *UAS-Katanin 60* insertion did not rescue this phenotype, whereas two copies of the *UAS-Katanin 60* insertion fully rescued the reduced QC in *Katanin 60*^{17A} mutants (Fig. 5G). The decreases in EJP amplitude, mEJP frequency and QC observed in *Katanin* mutants were all fully rescued by homozygous *UAS-Katanin 60* insertions (Fig. 5D,F,G), indicating that the neurotransmission defects are specifically caused by *Katanin 60* mutations.

Histone deacetylase 6 (*HDAC6*) antagonizes *Katanin 60* in regulating synaptic growth

A previous study on cultured mammalian cells reported that acetylated MTs are favored for severing by katanin (Sudo and Baas, 2010). HDAC6 deacetylates MTs in both mammals and *Drosophila* (Hubbert et al., 2002; Matsuyama et al., 2002; Sudo and Baas, 2010; Xiong et al., 2013). We confirmed the effects of HDAC6 on the MT acetylation by western analysis (Fig. 6J). To test whether the severing activity of Katanin is affected by MT acetylation status we examined genetic interactions between *Katanin 60* and *HDAC6* at NMJ synapses. Presynaptic overexpression of *Katanin 60* by *elav-Gal4* led to more satellite boutons compared with controls (*P*<0.001; Fig. 6A,B,I), whereas overexpression of *HDAC6* resulted in near-normal NMJ synapses (Fig. 6A,C,I). However, co-overexpression of *HDAC6* fully rescued the excess satellite boutons caused by *Katanin 60* overexpression (*P*<0.001; Fig. 6D,I). Postsynaptic overexpression of *Katanin 60* driven by *C57-Gal4* also led to more satellite boutons (*P*<0.001), although to a lower extent than with presynaptic overexpression of *Katanin 60* (Fig. 6B,F,I). Consistently, postsynaptic co-overexpression of *HDAC6* also completely rescued the excess of satellite boutons caused by *Katanin 60* overexpression, whereas postsynaptic overexpression of *HDAC6* alone did not affect synapse development (Fig. 6G-I). Together, these results demonstrate that HDAC6 antagonizes Katanin 60 in regulating NMJ development.

Negative regulation of dendritic arborization by *Katanin 60*

Microtubules play a crucial role in axon growth and dendritic morphogenesis (Conde and Cáceres, 2009; Jan and Jan, 2010; Jin et al., 2009; Sherwood et al., 2004). Immunostaining of third instar *Katanin 60* larvae, however, showed normal innervation of muscles by motor neurons, suggesting that motor neuron axon growth is largely normal. Furthermore, the axons of class IV dendritic arborization (da) neurons in the ventral nerve cord of *Katanin 60*-null or -overexpressing larvae showed no apparent abnormalities compared with wild-type larvae (data not shown).

The *Drosophila* da neurons provide an ideal system for studying dendritic morphogenesis. Four classes of da neurons can be distinguished according to their dendritic branching patterns and complexity, ranging from class I neurons with simple dendritic

Development (2014) doi:10.1242/dev.097774

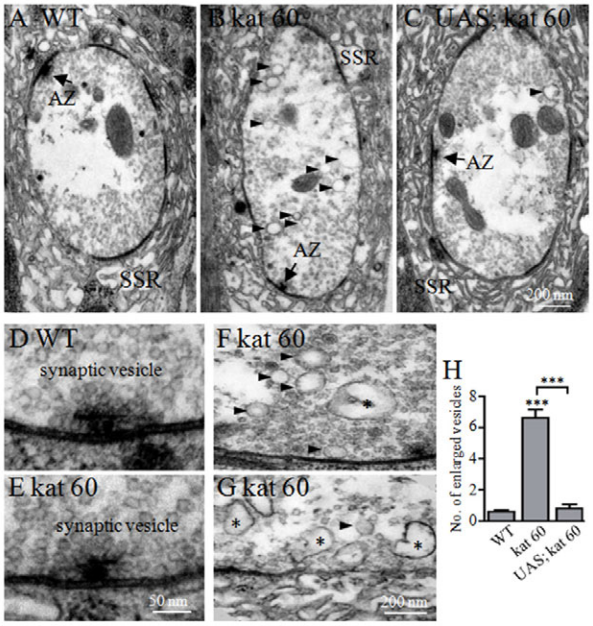

Fig. 4. Micrographs of synaptic boutons from different genotypes. (A-E) The genotypes are: (A) wild type, (B) *Katanin 60*^{17A} and (C) homozygous *UAS-Katanin 60* insertion in a *Katanin 60*^{17A} background. Subsynaptic reticulum (SSR) tightly surrounds the presynaptic bouton in the NMJ terminals. AZ, active zones (arrows). Arrowheads indicate enlarged cisternae in *Katanin 60*^{17A} mutants. (D,E) The features of active zones appear similar in wild type (D) and *Katanin*^{17A} (E). (F,G) There are more enlarged vesicles of up to 200 nm in diameter in *Katanin 60*^{17A} boutons. Asterisks indicate horse-shoe-shaped abnormal large vesicles. Arrowheads indicate enlarged vesicles. (H) Quantification of the number of large vesicles of ≥80 nm diameter in different genotypes. A total of 39 boutons from each genotype were analyzed. ***P<0.001.

arbors to class IV neurons with the most highly branched dendritic trees (Grueber et al., 2002; Jan and Jan, 2010). To investigate a possible role of Katanin in dendritic morphogenesis, we examined

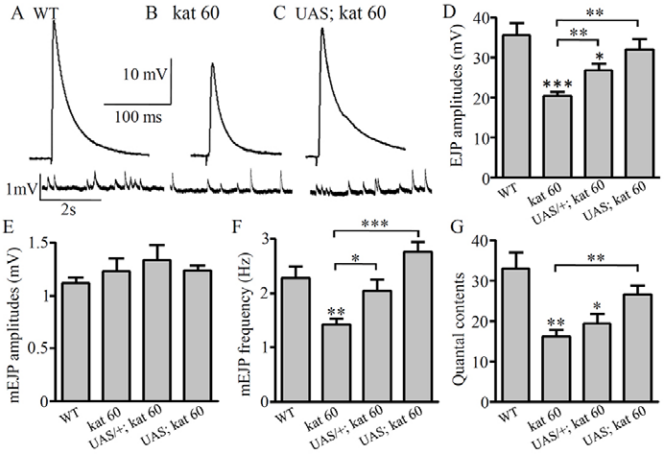

Fig. 5. EJP amplitude, mEJP frequency, and quantal content are reduced in *Katanin 60* mutant NMJ synapses. (A-C) Representative EJP (upper) and mEJP (lower) traces are shown for wild type (A), *Katanin 60*^{17A} (B) and *Katanin 60*^{17A} mutants carrying homozygous *UAS-Katanin 60* (C). All recordings were carried out on muscle 6 NMJ of the abdominal segment A3. (D-G) The differences in EJP amplitudes, mEJP amplitudes, mEJP frequencies and quantal contents in different genotypes (n=10, 9, 11 and 11 NMJs for the four genotypes, respectively). UAS, *UAS-Katanin 60* insertion. *P<0.05, **P<0.01, ***P<0.001.

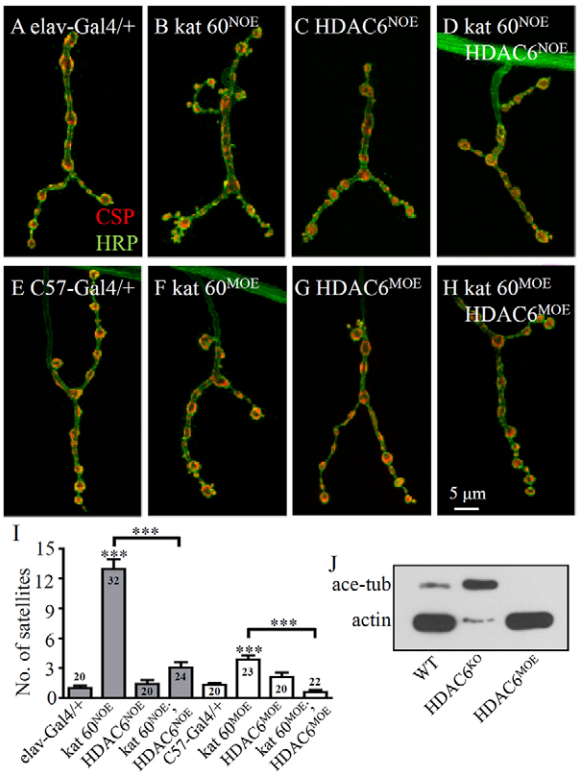

Fig. 6. *HDAC6* antagonizes *Katanin 60* in regulating synaptic growth. (A-H) Confocal images of muscle 4 NMJ synapses of abdominal segment A3 double-labeled with anti-CSP (red) and anti-HRP (green). Representative NMJ synapses of different genotypes are shown: control (*elav-Gal4*/+; A), neuronal overexpression (NOE) of *Katanin 60* (B) and *HDAC6* (C), and co-overexpression of *Katanin 60* and *HDAC6* (D) driven by *elav-Gal4*; control (*C57-Gal4*/+; E), muscular overexpression (MOE) of *Katanin 60* (F) and *HDAC6* (G), and co-overexpression of *Katanin 60* and *HDAC6* (H) driven by *C57-Gal4*. Scale bar: 5 μm. (I) Quantification of the number of the satellite boutons in different genotypes. Gray and white columns show antagonistic interactions between *Katanin 60* and *HDAC6* in presynaptic neurons and postsynaptic muscles, respectively. Comparisons were made between each genotype and its corresponding control by one-way ANOVA unless indicated otherwise. The number of NMJs analyzed for each genotype is given on the bars. ***P<0.001. Error bars indicate s.e.m. (J) HDAC6 negatively regulates the acetylation level of MTs. One tenth of the larval carcass proteins loaded for WT and HDAC6 overexpression was analyzed for HDAC6 nulls (HDAC6^{KO}). Actin was used as a loading control.

the dendritic elaboration of class IV neurons labeled by plasma membrane-bound GFP using the UAS-Gal4 system (*ppk-Gal4 >UAS-mCD8-GFP*). We quantified three dendritic features: dendrite field area, total dendritic length and number of termini. In *Katanin 60*^{17A} mutants the total dendritic length and the number of termini were significantly increased (Fig. 7A,B,G-I), whereas the dendrite field area of *Katanin 60* mutants showed no significant difference from the wild type. By contrast, overexpression of *Katanin 60* significantly reduced all three parameters (P<0.001; Fig. 7D,G-I). Importantly, the dendritic phenotypes of *Katanin 60*^{17A} mutants were fully rescued by Katanin 60 overexpression from the *UAS-Katanin 60* insertion (Fig. 7C,G-I). The rescue was confirmed using an independent non-targeted *UAS-Katanin 60* line.

To understand the effect of Katanin 60 on sensory neuron dendrites, we stained GFP-labeled class IV da neurons with anti-Futsch. Overexpression of *Katanin 60* significantly reduced the Futsch staining in cell bodies (P<0.001), axons (P<0.01) and dendrites (P<0.001) of class IV da neurons compared with the

Development (2014) doi:10.1242/dev.097774

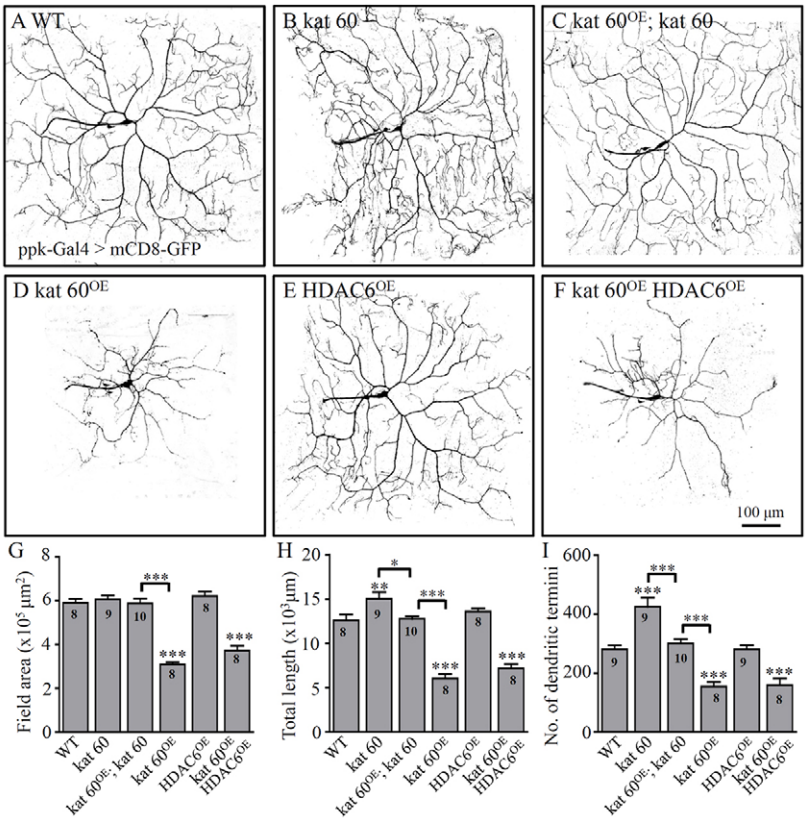

Fig. 7. Negative regulation of dendritic elaboration by *Katanin 60*. (A-F) Dendritic elaboration of class IV da neurons labeled with mCD8-GFP under the control of *ppk-GAL4*. The genotypes are: control (A), *Katanin 60*^{17A} (B), *Katanin 60* overexpression in *Katanin 60*^{17A} background (C), overexpression of *Katanin 60* (D) and *HDAC6* (E), and co-overexpression of *Katanin 60* and *HDAC6* (F) by *ppk-GAL4*. Scale bar: 100 μm. (G-I) Quantification of dendritic field area (G), the total dendritic length (H) and the number of dendritic termini (I) of various genotypes. *n*=8, 9, 10, 8, 8 and 8 neurons for the six genotypes, respectively. **P*<0.05, ***P*<0.01, ****P*<0.001. Error bars indicate s.e.m.

staining in the wild type (Fig. 8A,C), whereas *Katanin 60* knockdown by RNAi resulted in normal levels of Futsch staining in the three compartments of class IV da neurons (Fig. 8B,F).

To further understand the interaction between *Katanin 60* and *HDAC6* in dendritic morphogenesis, we co-overexpressed *Katanin 60* and *HDAC6*. Overexpression of *HDAC6* had no effect on dendritic elaboration (Fig. 7E,G-I). Unexpectedly, co-overexpression of *HDAC6* did not rescue the reduced dendritic elaboration caused by *Katanin 60* overexpression (Fig. 7D-I). Consistently, the reduced Futsch staining in dendrites, as well as in axons, caused by *Katanin 60* overexpression was not rescued by co-overexpression of HDAC6, though the reduced intensity of Futsch in the soma was fully rescued (Fig. 8C,E,F). The failure of HDAC6 co-overexpression to rescue the reduced dendritic elaboration may be caused by MT-independent toxicity conferred by *Katanin 60* overexpression. Alternatively, the antagonistic interaction between *Katanin 60* and *HDAC6* may not be effectively executed in dendrites, for unknown reasons. In any case, the genetic interaction between *Katanin 60* and *HDAC6* in regulating Futsch-positive MT levels in the neuronal soma is consistent with that in regulating NMJ development (Fig. 6) and MT network formation in muscle cells (see below).

HDAC6 antagonizes Katanin in regulating MT network formation in muscle cells

To define further the effects of HDAC6 on the severing ability of Katanin, we analyzed genetic interactions between Katanin 60 and HDAC6 by quantifying the intensities of perinuclear MT staining and the length of MT fibers in larval muscle cells, which are large and allow clear visualization of MT networks (Jin et al., 2009; Xiong et al., 2013; Yao et al., 2011). *Katanin 60*^{17A} mutant muscle cells had an unevenly distributed MT network and a significantly increased perinuclear MT intensity compared with wild-type cells (*P*<0.01; Fig. 9A,B,M). Overexpression of *Katanin 60* in muscles, however, dramatically decreased perinuclear MT density (*P*<0.001) with sparser and shorter MT fibers compared with wild-type muscles (Fig. 9A,C,M). Loss and gain of function of HDAC6 did not obviously alter the perinuclear MT network (Fig. 9A,D,E,M). As expected, co-overexpression of HDAC6 significantly rescued the decrease in MT density caused by *Katanin 60* overexpression (Fig. 9C,G,M). Conversely, the *HDAC6* null mutation enhanced the severing ability of overexpressed Katanin 60 because MT fibers were ~50% shorter than in Katanin 60-overexpressing muscles (*P*<0.001; Fig. 9C,F,N). We also analyzed genetic interactions between *HDAC6* and *spastin*; however, we found no effect of HDAC6 on the MT-severing ability of Spastin (Fig. 9I-N). Notably, overexpression of Katanin 60 produced longer MT fragments compared with that of Spastin (Fig. 9C,J), consistent with the effects of their respective mammalian counterparts on MTs in fibroblasts (Yu et al., 2008). Together, our genetic analyses revealed an antagonistic interaction between HDAC6 and Katanin, supporting the finding that Katanin but not Spastin exhibits enhanced severing of acetylated MTs.

HDAC6 has many substrates such as tubulin, cortactin and heat shock protein 90 (Valenzuela-Fernández et al., 2008). To investigate whether the tubulin deacetylase activity of HDAC6 was responsible for the protection of MTs from severing by Katanin 60, we tested genetic interactions when Katanin 60 and wild-type or mutated HDAC6 disrupting the deacetylase activities were co-overexpressed. The effect on MT severing was examined for two HDAC6 mutants with mutations in either of the two deacetylase domains (DD), H237A in DD1 and H664A in DD2 [the latter disrupts the tubulin deacetylase activity specifically (Xiong et al., 2013)]. We found that co-overexpression of the H237A mutant rescued the MT defects caused by *Katanin 60* overexpression as well as wild-type HDAC6, whereas the H664A mutant, expressed at similar levels as the H237A mutant (Xiong et al., 2013), did not (supplementary material

Development (2014) doi:10.1242/dev.097774

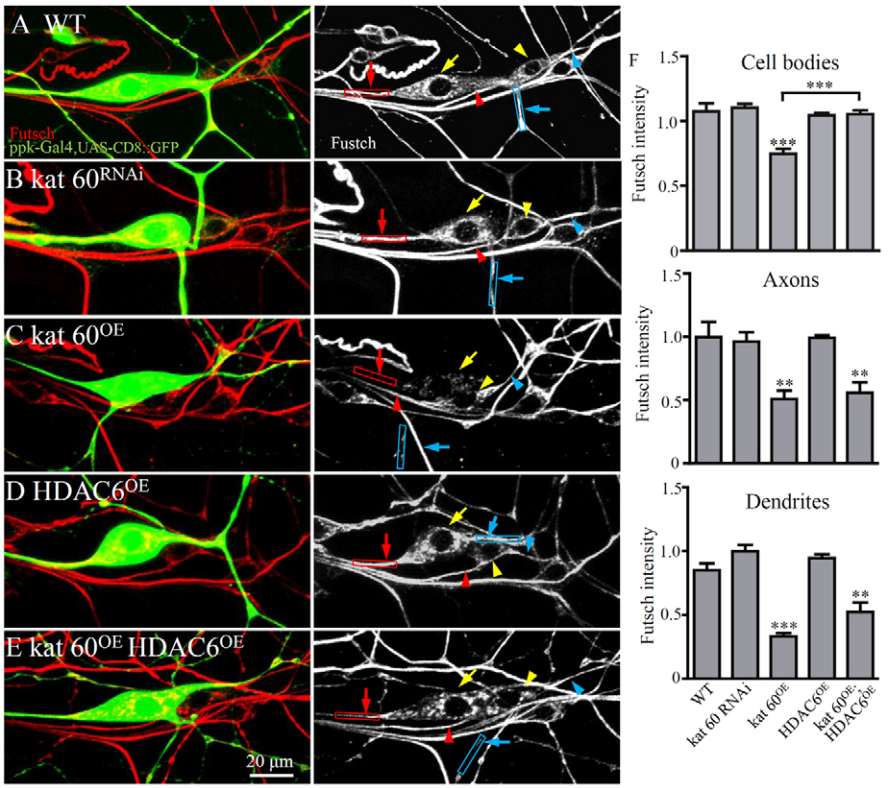

Fig. 8. *HDAC6* overexpression rescues the reduced Futsch staining caused by *Katanin 60* overexpression in the soma but not in proximal axons and dendrites of class IV da neurons. (A-E) Class IV da neurons labeled with mCD8-GFP (green) and co-stained with anti-Futsch (red). The genotypes are: control (A; *ppk-GAL4, UAS-mCD8-GFP/+*), *Katanin 60* RNAi (B), overexpression of *Katanin 60* (C) and *HDAC6* (D), and co-overexpression of *Katanin 60* and *HDAC6* (E) by *ppk-Gal4*. Cell bodies of class IV da neurons are indicated by yellow arrows, and those of the neighboring class I ddaF neuron, used as internal control, are indicated by yellow arrowheads. Axons and dendrites of class IV da neurons are indicated by red and blue arrows, respectively, whereas the axons and dendrites of class I ddaF neurons are indicated by red and blue arrowheads, respectively. Scale bar: 20 μm. (F) Statistical results of the Futsch staining intensity in the soma and 20 μm proximal axons and dendrites of class IV da neurons, normalized to the average intensities in the corresponding compartments of the neighboring class I ddaF neurons. Five pairs of neurons per genotype were analyzed. ***P*<0.01, ****P*<0.001. Error bars indicate s.e.m.

Fig. S3), confirming that reducing MT acetylation can protect MTs from Katanin severing.

DISCUSSION

Katanin 60 regulates NMJ synapse development

MTs have been shown to regulate the formation of dendritic spines, the postsynaptic structures of excitatory synapses in the mammalian brain (Penzes et al., 2009; Jaworski et al., 2009) and synapse growth at *Drosophila* NMJ terminals (Conde and Cáceres, 2009; Jin et al., 2009; Nahm et al., 2013; Wang et al., 2007; Yao et al., 2011; Zhang et al., 2001). We report here that mutations of *Katanin 60* resulted in more stable MT loops in the NMJ terminals (Fig. 3), contrasting with observations in *spastin* mutants in which MT loops were reduced and MTs depleted at the distal boutons (Sherwood et al., 2004). Consistently, *Katanin 60* and *spastin* regulate distinct aspects of NMJ growth, as *Katanin 60* and *spastin* double mutants showed a combined phenotype of the single mutants, i.e. more satellite boutons as in *Katanin 60* null mutants and more branches as in *spastin* null mutants (supplementary material Fig. S4).

Satellite boutons have been well documented in mutants with defects in endocytosis (Dickman et al., 2006), bone morphogenetic protein (BMP) signaling (O'Connor-Giles et al., 2008) and actin cytoskeleton dynamics (Coyle et al., 2004; Rodal et al., 2008; Ball et al., 2010). Because endocytosis attenuates BMP signaling and BMP signaling promotes F-actin formation by activating the expression of Trio, a guanine nucleotide exchange factor for Rac1, endocytosis-BMP-actin acts as an emerging pathway in regulating NMJ growth and bouton formation (Ball et al., 2010; O'Connor-Giles et al., 2008; Shi et al., 2013). The normal profile of synaptic vesicles at active zones (Fig. 4D,E), the normal amplitudes of mEJPs (Fig. 5) and the normal FM1-43 dye uptake and rundown under high-frequency stimulation (data not shown) indicate that *Katanin 60* probably does not affect synaptic endocytosis. How mutations in *Katanin 60* lead to the formation of excess satellite boutons remains to be elucidated.

Given that *Katanin 60* NMJ phenotypes were effectively rescued by leaky expression from the targeted *UAS-Katanin 60* insertion and the high sensitivity of neurons to Katanin 60 protein levels (Figs 2, 6), we were unable to address the tissue and/or cell type-specific requirements of Katanin 60 for NMJ growth. However, as presynaptic overexpression of *Katanin 60* in neurons produced pronounced NMJ abnormalities, whereas postsynaptic overexpression of *Katanin 60* in muscles only caused a mild NMJ phenotype (Fig. 6A,B,F,I), Katanin 60 may regulate NMJ synapse growth primarily in presynaptic neurons. Consistent with a presynaptic role of Katanin 60, *spastin* also acts presynaptically to regulate synaptic growth (Sherwood et al., 2004). Thus both *spastin* and *Katanin 60* normally suppress bouton formation at *Drosophila* NMJ terminals largely from the presynaptic neuron. In addition to similar NMJ morphological phenotypes, the neurotransmission efficiency (i.e. quantal content) was also reduced at NMJs of both *Katanin 60* and *spastin* mutants, again supporting a presynaptic function for both.

Katanin 60 negatively regulates dendritic elaboration

We demonstrate for the first time that Katanin 60 negatively regulates dendritic elaboration; *Katanin 60* mutations promote dendritic overgrowth, whereas overexpression of *Katanin 60* loss- and gain-of-function inhibits dendritic growth of class IV da neurons (Fig. 7). Furthermore, the opposite dendritic phenotypes of Katanin 60 loss- and gain-of-function mutants were mutually rescued to wild type (Fig. 7). The effects of Katanin 60 on dendritic elaboration are different from those of two other MT-severing proteins, Spastin and kat-60 L1. Both loss-of-function and gain-of-function of Spastin lead to reduced dendritic growth (Jinushi-Nakao et al., 2007; Ye et al., 2011), consistent with a previous report that mammalian spastin levels are important for neurite growth (Riano et al., 2009). In *kat-60 L1* mutants the dendritic field area and the number of the dendritic termini are significantly reduced, but the

Development (2014) doi:10.1242/dev.097774

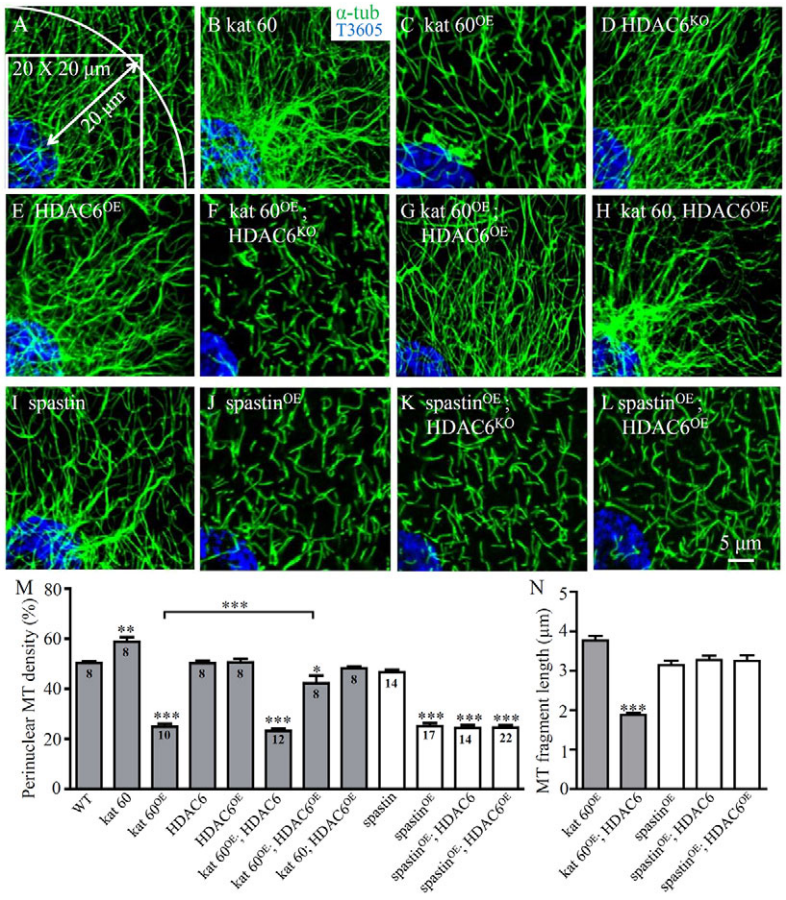

Fig. 9. HDAC6 antagonizes Katanin 60 in regulating MT network formation in muscle cells. (A-L) *Drosophila* larval muscles were co-stained with anti-α-tubulin to show the MT network (green) and T3605 to show the nucleus (blue) for wild type (A), *Katanin 60*^{17A} (B), *Katanin 60* overexpression by *C57-Gal4* (C), *HDAC6* null mutant (D), *HDAC6* overexpression by *C57-Gal4* (E), *Katanin 60* overexpression in a *HDAC6* null background (F), co-overexpression of *Katanin 60* and *HDAC6* by *C57-Gal4* (G), *HDAC6* overexpression in *Katanin 60*^{17A} background (H), *spastin*$^{5.75}$ (I), *spastin* overexpression by *C57-Gal4* (J), *spastin* overexpression in a *HDAC6* null background (K) and co-overexpression of *spastin* and *HDAC6* by *C57-Gal4* (L). Scale bar: 5 μm. (M) Quantification of α-tubulin staining intensities in the perinuclear area of muscle cells from different genotypes. The number of muscle cells analyzed for each genotype is given on the bars. (N) Quantification of MT fragment length. At least 120 MT fragments in the 20×20 μm square were analyzed from muscle cells of three animals of each genotype. **P*<0.05, ****P*<0.001.

effect of its overexpression on dendritic elaboration has not been documented (Stewart et al., 2012). Furthermore, kat-60 L1 preferentially severs MTs in the proximal dendrites of sensory neurons before dendritic detachment from the soma during metamorphosis (Lee et al., 2009). The apparent differential effects of different MT-severing proteins indicate that they regulate dendritic growth through distinct mechanisms. For example, the differences between katanin 60 and spastin may be due to their different subcellular localizations in the neuron. Spastin is enriched at growth cones, synapses and axonal branching points where extensive cytoskeletal remodeling occurs (Trotta et al., 2004; Yu et al., 2008), whereas katanin 60 is present in all regions of neurons (Karabay et al., 2004). The acetylation level of MTs and binding of MTs by various MAPs also differentially affect the severing activities of spastin and katanin 60 (see below).

Regulation of Katanin 60 activity and expression

Neurons contain high levels of Katanin compared with other cell types; without effective control the amount of Katanin 60 would theoretically be able to sever all MTs (McNally and Vale, 1993; Qiang et al., 2006). How are the MT-severing activity and expression of Katanin 60 regulated? It has been shown recently that the severing activity of Katanin 60 is regulated by phosphorylation, and phosphorylation of *Xenopus laevis* katanin 60 at serine 131 by Aurora B kinase was found to decrease its activity (Loughlin et al., 2011; Whitehead et al., 2013). In mammalian cells, the abundance of katanin 60 is regulated by Cul3/Klhdc5 E3 ligase, which mediates the ubiquitination and degradation of katanin 60 during mitosis (Cummings et al., 2009). By contrast, treatment of cultured hippocampal neurons with basic fibroblast growth factors increases the protein levels of katanin 60 and spastin, and consequently leads to the formation of excess axonal branches (Qiang et al., 2010). The expression of katanin 60 might also be regulated at the transcriptional level, as spastin expression is under tight transcriptional regulation (Jinushi-Nakao et al., 2007; Ye et al., 2011). Our results show that abnormal NMJs and disrupted MTs in neuronal soma and in muscle cells caused by Katanin 60 overexpression can be effectively rescued by co-overexpression of HDAC6 (Figs 6, 8, 9; supplementary material Fig. S3), in support of the conclusion from studies on cultured mammalian cells that katanin 60 preferentially severs acetylated MTs (Sudo and Baas, 2010). We note, however, that other phenotypes caused by Katanin 60 overexpression such as retarded dendritic elaboration and reduced MTs in axons and dendrites were not rescued by co-overexpression of HDAC6 (Figs 7, 8), suggesting that Katanin 60 overexpression may produce a MT-independent toxicity in neurites, or the antagonism between *HDAC6* and *Katanin 60* is subcellular compartment dependent, or both. In neurons, MTs are notably more acetylated in axons than in dendrites, but MTs in axons are protected by tau to resist severing by katanin (Sudo and Baas, 2010; Yu et al., 2008). Tau protection of MTs in axons from katanin-mediated severing is consistent with our observation that overexpression of Katanin 60 by *elav-Gal4* did not affect axonal growth (data not shown). How the activities of Katanin 60 are differentially regulated in different compartments of neurons remains to be determined.

MATERIALS AND METHODS

Drosophila stocks and husbandry

Flies were cultured on standard cornmeal medium at 25°C unless otherwise specified. w^{1118} was used as the wild-type control. Other stocks used included

Development (2014) doi:10.1242/dev.097774

muscle-specific *C57-Gal4* (Budnik et al., 1996), pan-neuronal *elav-Gal4*, ubiquitous *da-Gal4*, deficiency *Df(3R)ED5138*, which removes *Katanin 60* completely (all three from Bloomington Stock Center), and a GFP marker (*UAS-mCD8-GFP* under the control of *ppk-Gal4*) for class IV sensory neurons (Matthews et al., 2007). The *spastin*-null mutant *spastin*$^{5.75}$ was from N. Sherwood (Sherwood et al., 2004) and a *UAS-spastin* line was from K. Broadie (Trotta et al., 2004). The *HDAC6* null mutant (*HDAC6*^{KO}) and the *UAS-HDAC6* line were from R. Jiao (Du et al., 2010), and two UAS lines expressing mutant HDAC6 with mutation H237A or H664A in the two deacetylase domains were described previously (Xiong et al., 2013). An RNAi line of *Katanin 60* (v38369) was obtained from the Vienna *Drosophila* RNAi Center.

Knockout of *Katanin 60* by local hop and ends-out targeting

P-element-mediated excision was used to generate intragenic deletions in *Katanin 60* following a standard protocol. The original stock *EY09078* from Bloomington has a *P*-element insertion in the intergenic region between *Mms19* and *Katanin 60* (Fig. 1B). w^+ deletion lines in which the *P*-insertion was excised were initially screened by PCR followed by DNA sequencing, in conjunction with immunochemical analyses to confirm the mutations at the protein level (Fig. 1C).

For ends-out targeting of *Katanin 60*, the targeting donor DNA fragment contains 5′ and 3′ homologous arms flanking the target gene. The 5′ arm consisting of 2966 bp from 3R: 1058181 towards *Katanin 60* and the 3′ arm covering 3562 bp from 3R: 1049723 towards *Katanin 60* were cloned into the donor vector *pGX-attP* (Huang et al., 2008; Huang et al., 2009). The deletion mutants including *17A* were generated according to the protocol of Huang (Huang, 2008) and verified at DNA and protein levels (Fig. 1B-D).

Generation of UAS transgenic flies

For overexpression studies, a *UAS-Katanin 60* construct was made by cloning the full-length cDNA into the transformation vector *pUASTattB* (Bischof et al., 2007) and the commonly used *pUAST*. *pUASTattB-Katanin 60* was inserted into the second chromosome at 51D by site-directed integration using a specific stock *ZH-attP-51D* from the Bloomington Stock Center (BL24483), whereas *pUAST-Katanin 60* was inserted into chromosomes at non-targeted sites. The targeted insertion at 51D may express Katanin 60 ectopically because of an enhancer trap effect from the nearby *hibris* gene (http://flystocks.bio.indiana.edu/Reports/24483.html). Two independent, non-targeted UAS insertion lines, one in the second another in the third chromosome, were obtained. For overexpression and rescue experiments, we primarily used the targeted UAS insertion at 51D; in some cases, the results were verified by non-targeted insertions.

Immunochemical analyses and confocal microscopy

Western analysis was performed as described previously (Yao et al., 2011). Third instar larvae were dissected in PBS with all internal organs removed, followed by homogenization in a lysis buffer. Blots were first probed with primary antibodies: anti-Katanin 60 (1:500) against the N-terminal 264 amino acids of Katanin 60 (Zhang et al., 2007), anti-α-tubulin (1:50,000; mAb B-5-1-2; Sigma), anti-acetylated tubulin (1:5000; mAb 6-11B-1; Sigma) and anti-actin (1:50,000; mAb 1501; Chemicon), followed by incubation with HRP-coupled secondary antibodies. Protein bands were visualized by a chemiluminescence method (ECL Kit, Amersham).

Dissection and antibody staining of third instar larvae were performed as previously described (Jin et al., 2009; Yao et al., 2011). Primary antibodies included: anti-α-tubulin (1:1000; Sigma), rabbit anti-katanin 60 (1:50) (Zhang et al., 2007), Texas Red-conjugated goat anti-HRP (1:100; Jackson Laboratory), anti-Futsch [1:50; 22C10; the Developmental Studies Hybridoma Bank (DSHB) at the University of Iowa] and anti-cysteine string protein (CSP; 1:200; 6D6; DSHB). To examine the MT network in muscles, muscle 2 in abdominal segment A4 was analyzed because it has fewer tracheal branches to obscure the observation of MTs (Jin et al., 2009; Xiong et al., 2013). Nuclei were visualized by staining with TO-PRO(R) 3 iodide (T3605; 1:1000; Invitrogen) for 2 hours at room temperature. Images were collected with an Olympus FV10-ASW confocal microscope. The filament tracker tool of the Imaris software (Bitplane AG) was used to trace the staining signals from the confocal images (Fig. 3F-I). The green lines represent MT filaments detected with anti-tubulin, and the red lines outline neuronal membranes labeled with anti-HRP (Fig. 3F″-I″).

Quantifications of NMJ terminals were conducted largely following published procedures (Jin et al., 2009; Yao et al., 2011). All images analyzed were projections from complete *z*-stacks through the entire muscle 4 NMJ of the abdominal segment A3. Synaptic boutons were defined according to anti-HRP and anti-CSP (both label presynaptic components) staining.

To examine the role of Katanin in dendritic development, we labeled class IV sensory neurons with mCD8-GFP under the control of *ppk-Gal4* (Matthews et al., 2007). Confocal images of class IV dendritic arborization (da) neurons from abdominal segment 3 were analyzed with Imaris. The number of dendritic termini and the length of all dendritic branches were statistically analyzed (Jinushi-Nakao et al., 2007). The dendritic field area was defined by a polygon that connected the distal-most dendritic tips (Grueber et al., 2003).

Quantification of perinuclear MT density and MT fiber length in muscle cells, and Futsch staining intensity in class IV da neurons

Quantification of MT density in muscles was performed as previously described (Xiong et al., 2013). The perinuclear area was defined as the circular coverage that spans 20 μm around nuclei, which were visualized with T3605 staining. Tubulin staining signals within the perinuclear area from muscle 2 of abdominal segment A4 were calculated with ImageJ; the ratio of the tubulin-positive area to the perinuclear area was calculated automatically. The length of MT fragments was measured using ImageJ in a square of 20×20 μm as shown in Fig. 9A. For quantification of Futsch intensities in the cell bodies and 20 μm proximal axons or dendrites of class IV da neurons of the abdominal segment A3, staining signals were digitalized automatically using ImageJ and normalized to that of the neighboring control class I ddaF neurons without *ppk-Gal4* expression (Fig. 8).

Physiological assays

Intracellular recordings were carried out at 18°C following a conventional procedure. Specifically, wandering third instar larvae were dissected in Ca^{2+}-free HL3.1 saline (Feng et al., 2004; Jin et al., 2009) and recorded in HL3.1 saline containing 0.5 mM Ca^{2+}. Excitatory junctional potentials (EJPs) were recorded from muscle 6 of abdominal segment A3, followed by miniature EJP (mEJP) recording for 180 seconds. Quantal content was calculated by dividing the corrected EJP amplitude by the mEJP amplitude according to a classical protocol (Martin, 1955). The EJP correction for nonlinear summation was performed using a reversal potential of 10 mV.

Electron microscopy

Electron microscopy of NMJ terminals was performed largely according to previously published procedures (Liu et al., 2010; Liu et al., 2011; Zhao et al., 2013). Ultrathin (70-80 nm) longitudinal sections of NMJ 6 or 7 from the abdominal segment A3 were cut with a Leica UC6 ultramicrotome. Processed samples were observed under a JEOL 1400 electron microscope.

Statistical analyses

All statistical comparisons were performed using GraphPad InStat 5 software. *P*-values were calculated by one-way ANOVA. Comparisons were made between a specific genotype and the wild-type control (asterisks are located above a column) or between two specific genotypes (asterisks are located above a bracket).

Acknowledgements

We thank Drs K. Basler, K. Broadie, V. Budnik, Y. Hong, Y. N. Jan, R. J. Jiao, D. Sharp, N. Sherwood, the Bloomington Stock Center, the Vienna *Drosophila* RNAi Center and the Developmental Studies Hybridoma Bank, University of Iowa, for fly stocks, vectors, and antibodies. We thank Drs P. W. Baas, Z. H. Liu, N. T. Sherwood and B. Ye for discussions and comments on the manuscript and Dr L. Yang at the Microscopy Facility of our institute for electron microscopy analysis of NMJ synapses.

Competing interests

The authors declare no competing financial interests.

Author contributions

S.J. and Y.Q.Z. designed the project. C.M., Y.X., Z.X., Q.W. and S.J. performed the experiments. Y.Q.Z. and S.J. analyzed data and wrote the paper with inputs from C.M. and Y.X.

Funding

This work was supported by a grant from the Strategic Priority Research Program B of the Chinese Academy of Sciences [XDB02020400]; by grants from the National Science Foundation of China [31110103907 to Y.Q.Z.; and 81070909 and 31230045 to S.J.]. and by a grant from the State Key Laboratory of Molecular and Developmental Biology [2012-MDB-KF-07 to S.J.].

Supplementary material

Supplementary material available online at
http://dev.biologists.org/lookup/suppl/doi:10.1242/dev.097774/-/DC1

References

Ahmad, F. J., Yu, W., McNally, F. J. and Baas, P. W. (1999). An essential role for katanin in severing microtubules in the neuron. *J. Cell Biol.* **145**, 305-315.

Ball, R. W., Warren-Paquin, M., Tsurudome, K., Liao, E. H., Elazzouzi, F., Cavanagh, C., An, B. S., Wang, T. T., White, J. H. and Haghighi, A. P. (2010). Retrograde BMP signaling controls synaptic growth at the NMJ by regulating trio expression in motor neurons. *Neuron* **66**, 536-549.

Bischof, J., Maeda, R. K., Hediger, M., Karch, F. and Basler, K. (2007). An optimized transgenesis system for Drosophila using germ-line-specific phiC31 integrases. *Proc. Natl. Acad. Sci. USA* **104**, 3312-3317.

Blackstone, C., O'Kane, C. J. and Reid, E. (2011). Hereditary spastic paraplegias: membrane traffic and the motor pathway. *Nat. Rev. Neurosci.* **12**, 31-42.

Budnik, V., Koh, Y. H., Guan, B., Hartmann, B., Hough, C., Woods, D. and Gorczyca, M. (1996). Regulation of synapse structure and function by the Drosophila tumor suppressor gene dlg. *Neuron* **17**, 627-640.

Conde, C. and Cáceres, A. (2009). Microtubule assembly, organization and dynamics in axons and dendrites. *Nat. Rev. Neurosci.* **10**, 319-332.

Coyle, I. P., Koh, Y. H., Lee, W. C., Slind, J., Fergestad, T., Littleton, J. T. and Ganetzky, B. (2004). Nervous wreck, an SH3 adaptor protein that interacts with Wsp, regulates synaptic growth in Drosophila. *Neuron* **41**, 521-534.

Cummings, C. M., Bentley, C. A., Perdue, S. A., Baas, P. W. and Singer, J. D. (2009). The Cul3/Klhdc5 E3 ligase regulates p60/katanin and is required for normal mitosis in mammalian cells. *J. Biol. Chem.* **284**, 11663-11675.

Díaz-Valencia, J. D., Morelli, M. M., Bailey, M., Zhang, D., Sharp, D. J. and Ross, J. L. (2011). Drosophila katanin-60 depolymerizes and severs at microtubule defects. *Biophys. J.* **100**, 2440-2449.

Dickman, D. K., Lu, Z., Meinertzhagen, I. A. and Schwarz, T. L. (2006). Altered synaptic development and active zone spacing in endocytosis mutants. *Curr. Biol.* **16**, 591-598.

Du, G., Liu, X., Chen, X., Song, M., Yan, Y., Jiao, R. and Wang, C. C. (2010). Drosophila histone deacetylase 6 protects dopaminergic neurons against α-synuclein toxicity by promoting inclusion formation. *Mol. Biol. Cell* **21**, 2128-2137.

Feng, Y., Ueda, A. and Wu, C. F. (2004). A modified minimal hemolymph-like solution, HL3.1, for physiological recordings at the neuromuscular junctions of normal and mutant Drosophila larvae. *J. Neurogenet.* **18**, 377-402.

Grueber, W. B., Jan, L. Y. and Jan, Y. N. (2002). Tiling of the Drosophila epidermis by multidendritic sensory neurons. *Development* **129**, 2867-2878.

Grueber, W. B., Jan, L. Y. and Jan, Y. N. (2003). Different levels of the homeodomain protein cut regulate distinct dendrite branching patterns of Drosophila multidendritic neurons. *Cell* **112**, 805-818.

Hartman, J. J. and Vale, R. D. (1999). Microtubule disassembly by ATP-dependent oligomerization of the AAA enzyme katanin. *Science* **286**, 782-785.

Huang, J., Zhou, W., Watson, A. M., Jan, Y. N. and Hong, Y. (2008). Efficient ends-out gene targeting in Drosophila. *Genetics* **180**, 703-707.

Huang, J., Zhou, W., Dong, W., Watson, A. M. and Hong, Y. (2009). From the Cover: Directed, efficient, and versatile modifications of the Drosophila genome by genomic engineering. *Proc. Natl. Acad. Sci. USA* **106**, 8284-8289.

Hubbert, C., Guardiola, A., Shao, R., Kawaguchi, Y., Ito, A., Nixon, A., Yoshida, M., Wang, X. F. and Yao, T. P. (2002). HDAC6 is a microtubule-associated deacetylase. *Nature* **417**, 455-458.

Hummel, T., Krukkert, K., Roos, J., Davis, G. and Klämbt, C. (2000). Drosophila Futsch/22C10 is a MAP1B-like protein required for dendritic and axonal development. *Neuron* **26**, 357-370.

Jan, Y. N. and Jan, L. Y. (2010). Branching out: mechanisms of dendritic arborization. *Nat. Rev. Neurosci.* **11**, 316-328.

Jaworski, J., Kapitein, L. C., Gouveia, S. M., Dortland, B. R., Wulf, P. S., Grigoriev, I., Camera, P., Spangler, S. A., Di Stefano, P., Demmers, J. et al. (2009). Dynamic microtubules regulate dendritic spine morphology and synaptic plasticity. *Neuron* **61**, 85-100.

Jin, S., Pan, L., Liu, Z., Wang, Q., Xu, Z. and Zhang, Y. Q. (2009). Drosophila Tubulin-specific chaperone E functions at neuromuscular synapses and is required for microtubule network formation. *Development* **136**, 1571-1581.

Jinushi-Nakao, S., Arvind, R., Amikura, R., Kinameri, E., Liu, A. W. and Moore, A. W. (2007). Knot/Collier and cut control different aspects of dendrite cytoskeleton and synergize to define final arbor shape. *Neuron* **56**, 963-978.

Karabay, A., Yu, W., Solowska, J. M., Baird, D. H. and Baas, P. W. (2004). Axonal growth is sensitive to the levels of katanin, a protein that severs microtubules. *J. Neurosci.* **24**, 5778-5788.

Lee, H. H., Jan, L. Y. and Jan, Y. N. (2009). Drosophila IKK-related kinase Ik2 and Katanin p60-like 1 regulate dendrite pruning of sensory neuron during metamorphosis. *Proc. Natl. Acad. Sci. USA* **106**, 6363-6368.

Liu, Z., Chen, Y., Wang, D., Wang, S. and Zhang, Y. Q. (2010). Distinct presynaptic and postsynaptic dismantling processes of Drosophila neuromuscular junctions during metamorphosis. *J. Neurosci.* **30**, 11624-11634.

Liu, Z., Huang, Y., Zhang, Y., Chen, D. and Zhang, Y. Q. (2011). Drosophila Acyl-CoA synthetase long-chain family member 4 regulates axonal transport of synaptic vesicles and is required for synaptic development and transmission. *J. Neurosci.* **31**, 2052-2063.

Loughlin, R., Wilbur, J. D., McNally, F. J., Nédélec, F. J. and Heald, R. (2011). Katanin contributes to interspecies spindle length scaling in Xenopus. *Cell* **147**, 1397-1407.

Martin, A. R. (1955). A further study of the statistical composition on the end-plate potential. *J. Physiol.* **130**, 114-122.

Matsuyama, A., Shimazu, T., Sumida, Y., Saito, A., Yoshimatsu, Y., Seigneurin-Berny, D., Osada, H., Komatsu, Y., Nishino, N., Khochbin, S. et al. (2002). In vivo destabilization of dynamic microtubules by HDAC6-mediated deacetylation. *EMBO J.* **21**, 6820-6831.

Matthews, B. J., Kim, M. E., Flanagan, J. J., Hattori, D., Clemens, J. C., Zipursky, S. L. and Grueber, W. B. (2007). Dendrite self-avoidance is controlled by Dscam. *Cell* **129**, 593-604.

McNally, F. J. and Vale, R. D. (1993). Identification of katanin, an ATPase that severs and disassembles stable microtubules. *Cell* **75**, 419-429.

Nahm, M., Lee, M. J., Parkinson, W., Lee, M., Kim, H., Kim, Y. J., Kim, S., Cho, Y. S., Min, B. M., Bae, Y. C. et al. (2013). Spartin regulates synaptic growth and neuronal survival by inhibiting BMP-mediated microtubule stabilization. *Neuron* **77**, 680-695.

O'Connor-Giles, K. M., Ho, L. L. and Ganetzky, B. (2008). Nervous wreck interacts with thickveins and the endocytic machinery to attenuate retrograde BMP signaling during synaptic growth. *Neuron* **58**, 507-518.

Ozdowski, E. F., Gayle, S., Bao, H., Zhang, B. and Sherwood, N. T. (2011). Loss of Drosophila melanogaster p21-activated kinase 3 suppresses defects in synapse structure and function caused by spastin mutations. *Genetics* **189**, 123-135.

Penzes, P., Srivastava, D. P. and Woolfrey, K. M. (2009). Not just actin? A role for dynamic microtubules in dendritic spines. *Neuron* **61**, 3-5.

Qiang, L., Yu, W., Andreadis, A., Luo, M. and Baas, P. W. (2006). Tau protects microtubules in the axon from severing by katanin. *J. Neurosci.* **26**, 3120-3129.

Qiang, L., Yu, W., Liu, M., Solowska, J. M. and Baas, P. W. (2010). Basic fibroblast growth factor elicits formation of interstitial axonal branches via enhanced severing of microtubules. *Mol. Biol. Cell* **21**, 334-344.

Riano, E., Martignoni, M., Mancuso, G., Cartelli, D., Crippa, F., Toldo, I., Siciliano, G., Di Bella, D., Taroni, F., Bassi, M. T. et al. (2009). Pleiotropic effects of spastin on neurite growth depending on expression levels. *J. Neurochem.* **108**, 1277-1288.

Rodal, A. A., Motola-Barnes, R. N. and Littleton, J. T. (2008). Nervous wreck and Cdc42 cooperate to regulate endocytic actin assembly during synaptic growth. *J. Neurosci.* **28**, 8316-8325.

Roll-Mecak, A. and McNally, F. J. (2010). Microtubule-severing enzymes. *Curr. Opin. Cell Biol.* **22**, 96-103.

Roos, J., Hummel, T., Ng, N., Klämbt, C. and Davis, G. W. (2000). Drosophila Futsch regulates synaptic microtubule organization and is necessary for synaptic growth. *Neuron* **26**, 371-382.

Ruiz-Canada, C., Ashley, J., Moeckel-Cole, S., Drier, E., Yin, J. and Budnik, V. (2004). New synaptic bouton formation is disrupted by misregulation of microtubule stability in aPKC mutants. *Neuron* **42**, 567-580.

Sharma, N., Bryant, J., Wloga, D., Donaldson, R., Davis, R. C., Jerka-Dziadosz, M. and Gaertig, J. (2007). Katanin regulates dynamics of microtubules and biogenesis of motile cilia. *J. Cell Biol.* **178**, 1065-1079.

Sharp, D. J. and Ross, J. L. (2012). Microtubule-severing enzymes at the cutting edge. *J. Cell Sci.* **125**, 2561-2569.

Sherwood, N. T., Sun, Q., Xue, M., Zhang, B. and Zinn, K. (2004). Drosophila spastin regulates synaptic microtubule networks and is required for normal motor function. *PLoS Biol.* **2**, e429.

Shi, W., Chen, Y., Gan, G., Wang, D., Ren, J., Wang, Q., Xu, Z., Xie, W. and Zhang, Y. Q. (2013). Brain tumor regulates neuromuscular synapse growth and endocytosis in Drosophila by suppressing mad expression. *J. Neurosci.* **33**, 12352-12363.

Srayko, M., O'Toole, E. T., Hyman, A. A. and Müller-Reichert, T. (2006). Katanin disrupts the microtubule lattice and increases polymer number in C. elegans meiosis. *Curr. Biol.* **16**, 1944-1949.

Stewart, A., Tsubouchi, A., Rolls, M. M., Tracey, W. D. and Sherwood, N. T. (2012). Katanin p60-like1 promotes microtubule growth and terminal dendrite stability in the larval class IV sensory neurons of Drosophila. *J. Neurosci.* **32**, 11631-11642.

Sudo, H. and Baas, P. W. (2010). Acetylation of microtubules influences their sensitivity to severing by katanin in neurons and fibroblasts. *J. Neurosci.* **30**, 7215-7226.

Trotta, N., Orso, G., Rossetto, M. G., Daga, A. and Broadie, K. (2004). The hereditary spastic paraplegia gene, spastin, regulates microtubule stability to modulate synaptic structure and function. *Curr. Biol.* **14**, 1135-1147.

Vale, R. D. (1991). Severing of stable microtubules by a mitotically activated protein in Xenopus egg extracts. *Cell* **64**, 827-839.

Valenzuela-Fernández, A., Cabrero, J. R., Serrador, J. M. and Sánchez-Madrid, F. (2008). HDAC6: a key regulator of cytoskeleton, cell migration and cell-cell interactions. *Trends Cell Biol.* **18**, 291-297.

Wang, X., Shaw, W. R., Tsang, H. T., Reid, E. and O'Kane, C. J. (2007). Drosophila spichthyin inhibits BMP signaling and regulates synaptic growth and axonal microtubules. *Nat. Neurosci.* **10**, 177-185.

Whitehead, E., Heald, R. and Wilbur, J. D. (2013). N-terminal phosphorylation of p60 katanin directly regulates microtubule severing. *J. Mol. Biol.* **425**, 214-221.

Xiong, Y., Zhao, K., Wu, J., Xu, Z., Jin, S. and Zhang, Y. Q. (2013). HDAC6 mutations rescue human tau-induced microtubule defects in Drosophila. *Proc. Natl. Acad. Sci. USA* **110**, 4604-4609.

Yao, A., Jin, S., Li, X., Liu, Z., Ma, X., Tang, J. and Zhang, Y. Q. (2011). Drosophila FMRP regulates microtubule network formation and axonal transport of mitochondria. *Hum. Mol. Genet.* **20**, 51-63.

Ye, B., Kim, J. H., Yang, L., McLachlan, I., Younger, S., Jan, L. Y. and Jan, Y. N. (2011). Differential regulation of dendritic and axonal development by the novel Krüppel-like factor Dar1. *J. Neurosci.* **31**, 3309-3319.

Yu, W., Qiang, L., Solowska, J. M., Karabay, A., Korulu, S. and Baas, P. W. (2008). The microtubule-severing proteins spastin and katanin participate differently in the formation of axonal branches. *Mol. Biol. Cell* **19**, 1485-1498.

Zhang, Y. Q., Bailey, A. M., Matthies, H. J., Renden, R. B., Smith, M. A., Speese, S. D., Rubin, G. M. and Broadie, K. (2001). Drosophila fragile X-related gene regulates the MAP1B homolog Futsch to control synaptic structure and function. *Cell* **107**, 591-603.

Zhang, D., Rogers, G. C., Buster, D. W. and Sharp, D. J. (2007). Three microtubule severing enzymes contribute to the "Pacman-flux" machinery that moves chromosomes. *J. Cell Biol.* **177**, 231-242.

Zhang, D., Grode, K. D., Stewman, S. F., Diaz-Valencia, J. D., Liebling, E., Rath, U., Riera, T., Currie, J. D., Buster, D. W., Asenjo, A. B. et al. (2011). Drosophila katanin is a microtubule depolymerase that regulates cortical-microtubule plus-end interactions and cell migration. *Nat. Cell Biol.* **13**, 361-369.

Zhao, L., Wang, D., Wang, Q., Rodal, A. A. and Zhang, Y. Q. (2013). Drosophila cyfip regulates synaptic development and endocytosis by suppressing filamentous actin assembly. *PLoS Genet.* **9**, e1003450.

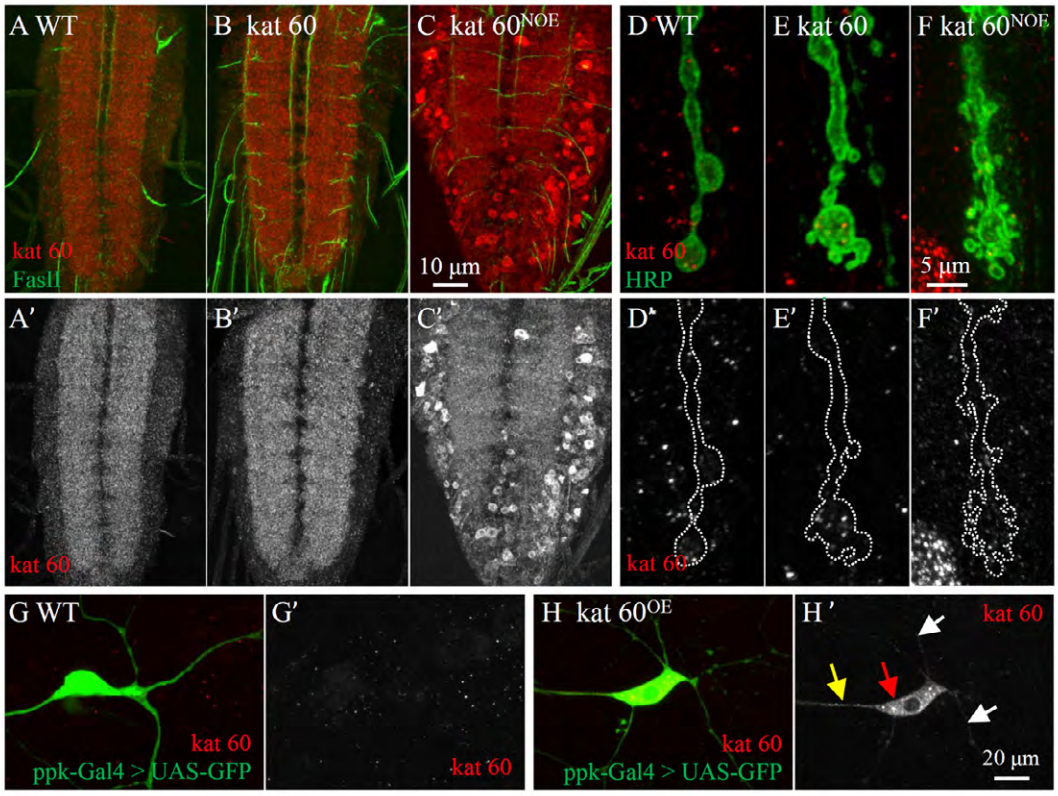

Fig. S1. No endogenous katanin 60 is detected in the ventral nerve cord and class IV da sensory neurons of third instar larvae. No specific expression of endogenous katanin 60 was observed in the ventral nerve cord (VNC) (A,A',B,B'), NMJs (D,D',E,E') and da neurons (G,G') of third instar larvae. When katanin 60 was overexpressed under the control of the pan-neuronal *elav-Gal4*, prominent accumulation of katanin 60 was observed in the soma of VNC neurons (C,C'), but no specific enrichment of katanin 60 was observed in axons (A-C,A'-C') and NMJs (F,F'). Axons were labeled with anti-fasciclin II (FasII). When katanin 60 was overexpressed in class IV da neurons under the control of *ppk-Gal4*, it was evenly distributed in all compartments including soma (red arrow), axons (yellow arrow), and dendrites (white arrow) (H,H'). Scale bars in C, F, and H' represent 10, 5, and 20 µm, respectively.

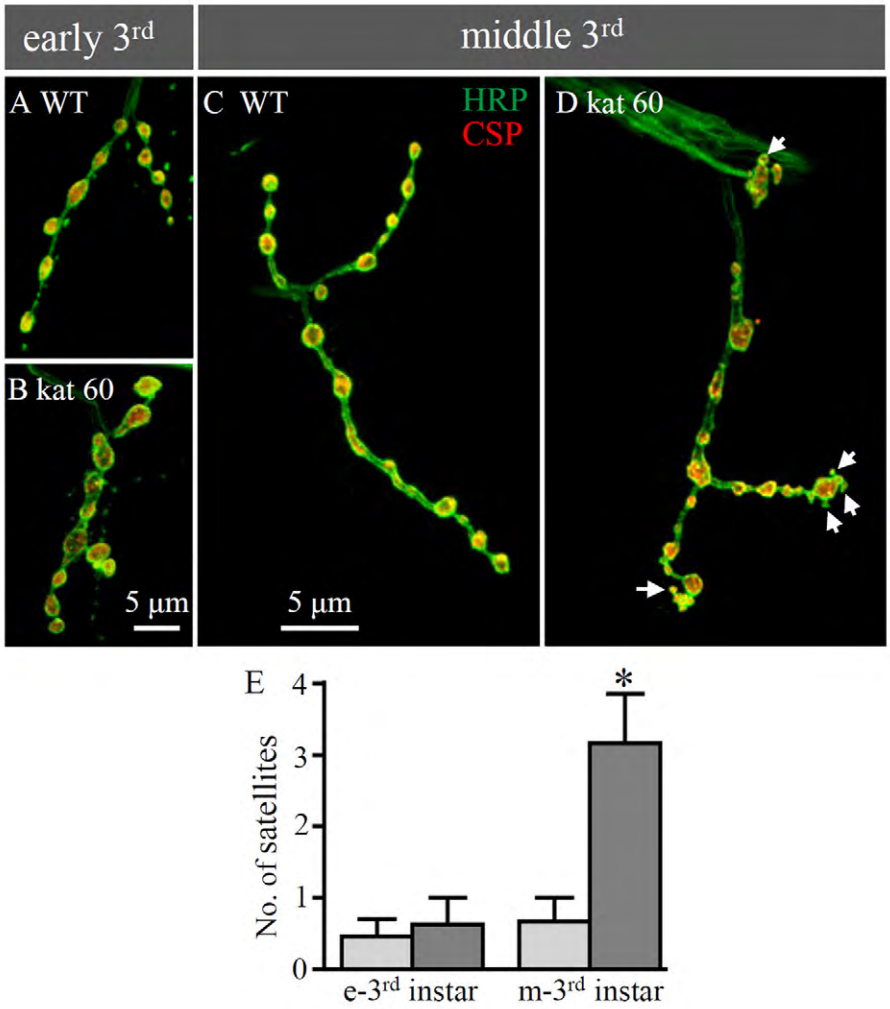

Fig. S2. Satellite boutons form in the middle third instar larval stages of *katanin 60* mutants. (**A-D**) Representative NMJ4 synapses from different third instar larval stages. Early third (e-3rd; A,B) and middle third (m-3rd; C,D) instar larvae were double-stained with anti-HRP (green) and anti-CSP (red). Larval stages were determined according to the developmental timing, the structure of mouth hook, and the appearance of anterior spiracles. Satellite boutons appear in the middle 3rd instar larval stages in *katanin* 60^{17A} mutants (D). Arrows indicate satellite boutons in D. Scale bars in B and C denote 5 μm. (**E**) Quantification results of the number of satellite boutons in different developmental stages. In *katanin* 60^{17A} mutants, the number of satellite boutons increased in the middle 3rd instar compared with wild type (n=8 for each genotype). *P<0.05. Error bars indicate s.e.m.

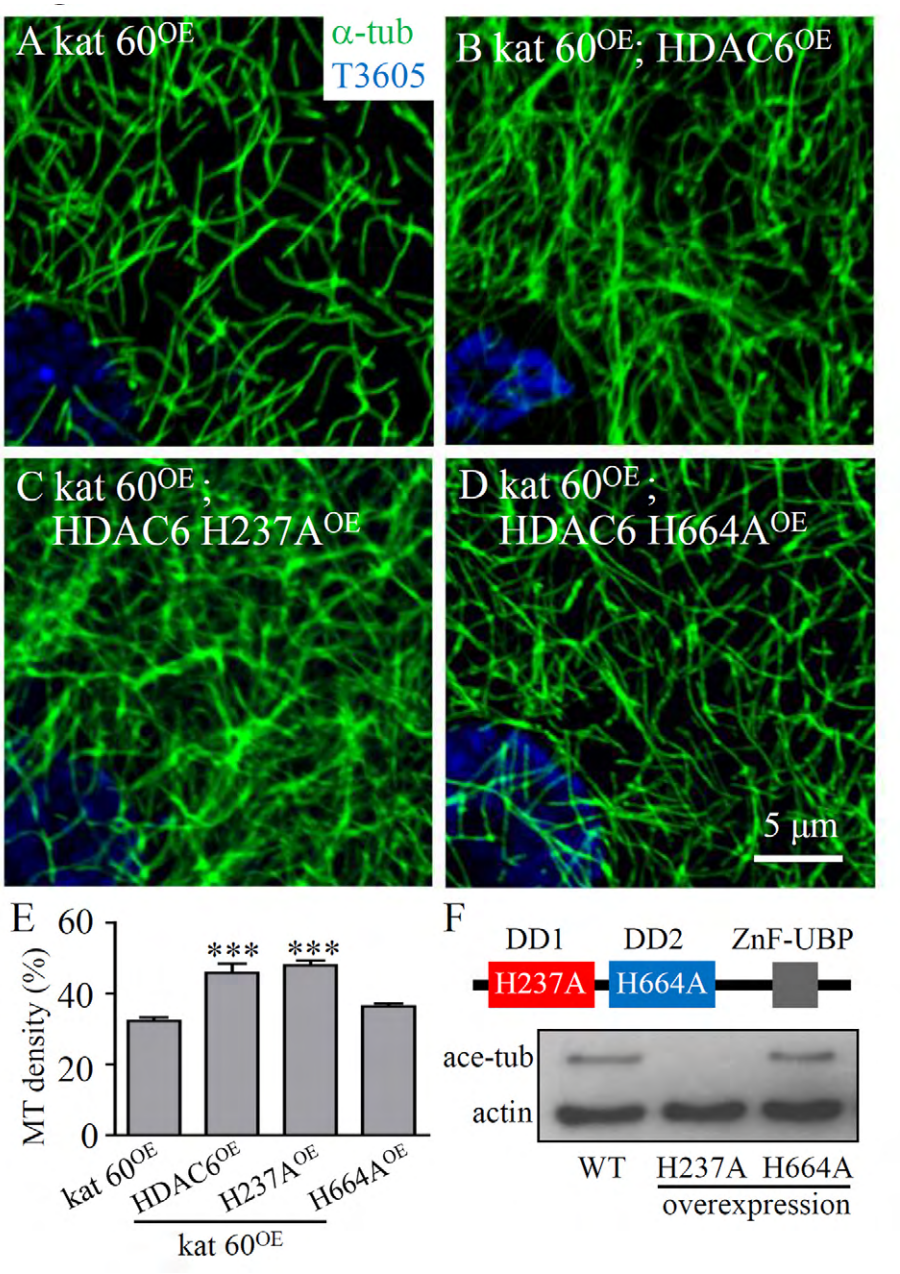

Fig S3. The tubulin specific deacetylase activity of HDAC6 is responsible for the rescue of katanin 60-induced MT defects. (**A-D**) Representative images of perinuclear MTs of larval muscles stained with anti-α-tubulin to show the MT network (green) and with T3605 to show the nucleus (blue). Overexpression of H237A (C) but not H664A mutant (D) HDAC6 rescued katanin 60-induced MT defects (A) as wild-type HDAC6 (B). Scale bar in D, 5 μm. (**E**) Quantification results of perinuclear MT densities of different genotypes (n=6). ***P<0.001. Error bars indicate s.e.m. (**F**) HDAC6 domain organization (upper panel). DD1 and DD2 indicate deacetylase domains 1 and 2, respectively. ZnF–UBP denotes zinc-finger ubiquitin binding domain. Western analysis (lower panel) demonstrated that overexpression of H237A mutant HDAC6 decreases the acetylation level of MTs, whereas that of H664A mutant HDAC6 does not.

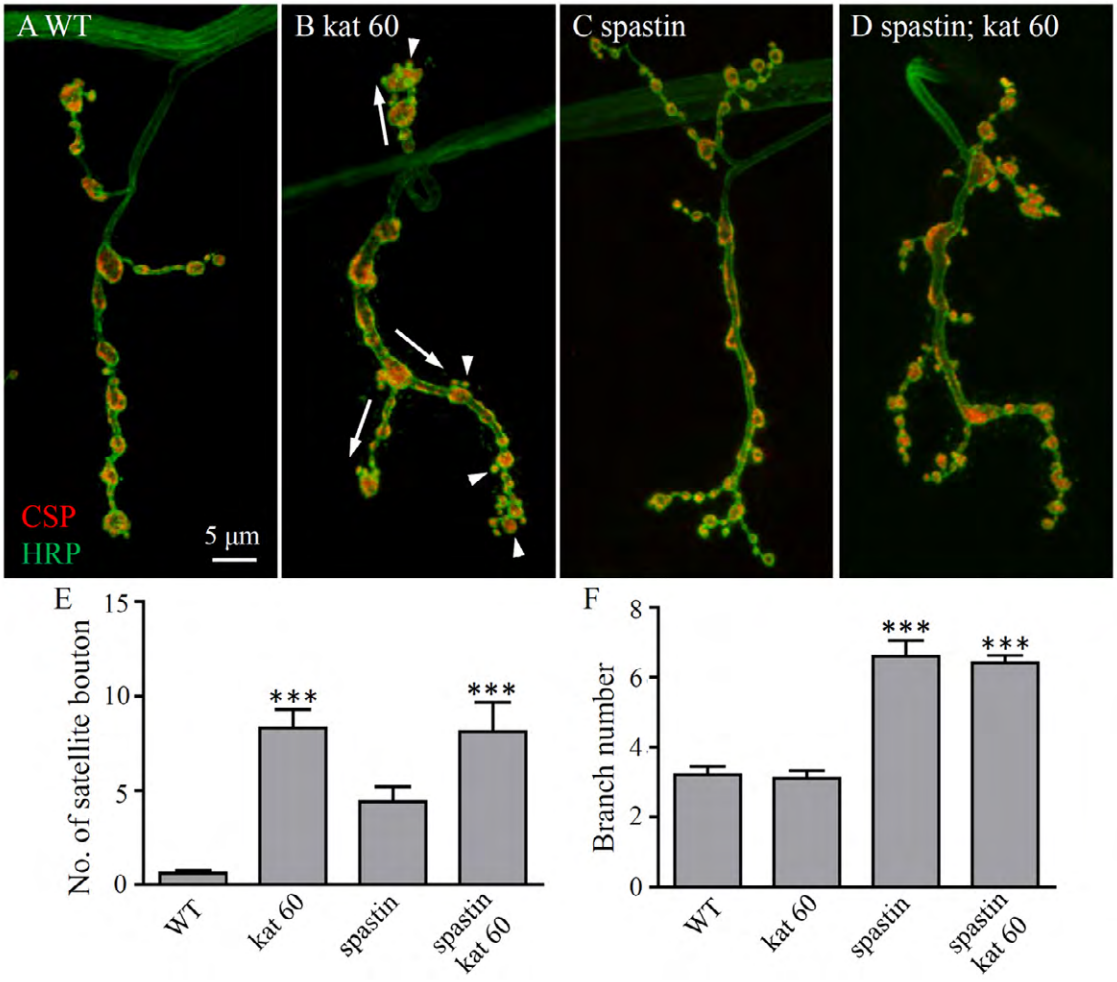

Fig. S4. *spastin* and *katanin 60* regulate distinct aspects of NMJ growth. NMJs from wandering third instar larvae were double-stained with anti-HRP (green) and anti-CSP (red) detecting the neuronal membrane and synaptic vesicles, respectively. (**A-D**) Representative muscle 4 NMJs in the abdominal segment A3 from wild-type control (A), *katanin* 60^{17A} null mutant (B), *spastin*$^{5.75}$ null mutant (C), and *spastin katanin 60* double mutant (D) are shown. Arrowheads indicate satellite boutons; arrows denote synaptic branches in B. Scale bar in A, 5 µm. (**E**, **F**) Quantification of the number of satellite boutons (E) and branches (F) from different genotypes (n=10 NMJs). Branches originating directly from the nerve entry point were defined as primary branches, and each higher-order branch was counted only when two or more boutons in a string could be observed (Jin et al., 2009). ***P<0.001. Error bars indicate s.e.m.